Published in final edited form as:
J Mol Biol. 2009 September 11; 392(1): 143–153. doi:10.1016/j.jmb.2009.06.079.

Crystal Structure of Miner1: The Redox Active 2Fe-2S Protein Causative in Wolfram Syndrome 2

Andrea R. Conlan[*], **Herbert L. Axelrod**[†], **Aina E. Cohen**[†], **Edward C. Abresch**[‡], **John Zuris**[*], **David Yee**[‡], **Rachel Nechushtai**[§], **Patricia A. Jennings**[*,**], and **Mark L. Paddock**[‡,**]

[*] Department of Chemistry and Biochemistry, University of California at San Diego, La Jolla, CA 92093

[‡] Department of Physics, University of California at San Diego, La Jolla, CA 92093

[†] Stanford Synchrotron Radiation Laboratory, 2575 Sand Hill Road, Menlo Park, CA 94025

[§] Department of Plant and Environmental Sciences, The Wolfson Centre for Applied Structural Biology, Hebrew University of Jerusalem, Givat Ram 91904, Israel

Abstract

The endoplasmic reticulum protein Miner1 is essential for health and longevity. Mis-splicing of CISD2, which codes for Miner1, is causative in Wolfram Syndrome 2 (WFS2) resulting in early onset optic atrophy, diabetes mellitus, deafness and decreased lifespan. In knock-out studies, disruption of CISD2 leads to accelerated aging, blindness and muscle atrophy. In this work, we characterized the soluble region of human Miner1 and solved its crystal structure to a resolution of 2.1 Å (R-factor=17%). Although originally annotated as a zinc finger, we show that Miner1 is a homodimer harboring two redox active 2Fe-2S clusters indicating for the first time an association of a redox active FeS protein with WFS2. Each 2Fe-2S cluster is bound by a rare 3Cys-1His motif within a 17 amino acid segment. Miner1 is the first functionally different protein that shares the unique NEET fold similar of its recently identified paralog mitoNEET, an outer mitochondrial membrane protein. We also report the first measurement of the redox potentials (E_m) of Miner1 and mitoNEET showing that they are proton-coupled with $E_m \sim 0$ mV at pH 7.5. Changes in the pH sensitivity of their cluster stabilities are attributed to significant differences in the electrostatic distribution and surfaces between the two proteins. The structural and biophysical results are discussed in relation to possible roles of Miner1 in cellular Fe-S management and redox reactions.

Keywords

diabetes; membrane bound; oxidative stress; CDGSH; ER stress

**To whom correspondence should be addressed at: Department of Physics, University of California at San Diego, 9500 Gilman Drive, La Jolla, CA 92093-0319, e-mail: mpaddock@ucsd.edu; To whom correspondence should be addressed at: Department of Chemistry and Biochemistry, University of California at San Diego, 9500 Gilman Drive, La Jolla, CA 92093-0375, e-mail: pajennings@ucsd.edu.

Introduction

Miner1 [¶], originally annotated as a zinc finger protein of unknown function, is actually a unique redox active Fe-S protein. The gene encoding Miner1, CISD2 (CDGSH iron sulfur domain 2),[‖] found at chromosomal location 4q24, was recently identified as the carrier of a mutation that causes Wolfram Syndrome 2 (WFS2) [1]. The pre-mRNA of CISD2 has two splice sites, creating 3 exons and 2 introns (Fig. 1). Correct splicing is essential for the proper translation and function of Miner1. It localizes to the endoplasmic reticulum (ER) when properly expressed and folded. The mutation found in WFS2 patients is a G to C base pair transversion in pre-mRNA CISD2 that causes a splicing error resulting in removal of the second exon and introduction of a premature stop codon, that eliminate 75% of the protein transcript (Fig. 1) [1]. Indeed, the region binding the 2Fe-2S cluster is completely eliminated. Although initially healthy, patients with WFS2 experience a decreased life expectancy, early onset diabetes mellitus, optical atrophy, sensorineural deafness, and a significant bleeding tendency [1]. Thus, studies of structure and function of Miner1 are expected to provide critical information on the fundamental cause of the disease and reasons for the decrease in life expectancy.

CISD2 lies on chromosome 4, a genetic locus associated with longevity. Investigations focused on the longevity locus where researchers disrupted CISD2 in mice found that the elimination of Miner1 resulted in decreased life expectancy and reduced general health [2]. These knockout mice show accelerated aging, blindness, an abnormal skeleton, and muscle atrophy [2], effects that are very similar to those described in the WFS2 patients. The mouse ortholog is 96% identical to the human Miner1 and is highly conserved (94–100%) with other mammals (supplemental Fig. S1). Obtaining the Miner1 protein structure provides a basis for understanding functional consequences of mutations in human and animal studies.

Miner1 belongs to a newly discovered family, which includes the 2Fe-2S containing outer mitochondrial membrane (OMM) protein mitoNEET [3; 4]. In contrast, Miner1 localizes to the ER [1]. It contains an atypical ER localization sequence, an N-terminal transmembrane domain, and a CDGSH 2Fe-2S domain. To facilitate yields and structural studies, we focused on the soluble domain of the protein and made a point mutation at the only non-conserved free cysteine (supplemental Fig. S1). In this work, we show that the Cys mutation does not affect the properties and report the crystal structure of the soluble region of Miner1 (C92S) solved at 2.1 Å resolution using Fe-MAD phasing [5]. The structure is homodimeric with a scaffold similar to the OMM protein mitoNEET, but has a distinct surface topology and differences in the charge distribution. We also report and compare redox and stability measurements as functions of pH for both Miner1 and its paralog mitoNEET [6].

Results

Isolation and UV-Vis Spectroscopy of the ER protein Miner1

In an effort to understand the properties of this protein we produced a soluble form of recombinant human Miner1 that corresponds to amino acids 57-135 (lacking the amino-terminal targeting and transmembrane sequences). The protein was fused to a cleavable His-tag to facilitate purification. As a result, the construct includes an additional four amino acids (GSHM) at the N-terminus. Early attempts at purification were hindered by protein instability and aggregation. Although use of reducing agent decreased aggregation, yields remained insufficient for structural studies. Therefore, we replaced the one free nonconserved cysteine (Supplemental Fig. S1) with the isosteric serine (C92S). The resultant mutant protein, Miner1 (C92S), has the same optical signature of the native Miner1 (Fig. 2). Furthermore, the construct

[¶]Also known as ERIS, CDGSH2
[‖]Previous symbol ZCD2

had the desirable effects of improved yields of purified protein and a decreased tendency to aggregate. Since the point mutation does not change the spectra of Miner1, we will refer to Miner1(C92S) as Miner1 hereon.

The Overall Fold of Miner1

The isolated purified recombinant protein showed CD spectra (Fig. S2) indicative of a well folded protein with a chiral center. The protein was amenable to crystallization. X-ray diffraction intensities were collected at Stanford Synchrotron Radiation Laboratory (SSRL) BL7-1 and BL9-2 to 2.1 Å (Table 1). Miner1 crystallized in the orthorhombic space group $P2_12_12_1$ with unit-cell parameters a =49.90 Å, b=48.58 Å, c=74.10 Å, α=β=γ=90° (Table 1). The Matthews coefficient (V_m) of the crystal was 2.0 $Å^3$/Dalton with an estimated solvent content of 37%.

Experimental phases for model building were determined by using Fe-MAD [5]. The model was refined using 2.1 Å data to an R-factor of 17.0% (R_{free}=21.6%). The high quality of the electron density is shown in Fig. 3A. The refined model reveals a parallel homodimeric structure that includes the cytoplasmic fragment of each protomer from Asp68 to Glu134 on Protomer A and to Val135 on Protomer B (Fig. 3A). Fifteen amino acids at the N-termini are disordered and not resolved in the electron density. The homodimer is tightly packed with 1800 $Å^2$ of buried surface area at the interface as calculated using PISA [7]. Model validation using the MOLPROBITY [8] structure validation tool indicates that 97% of the amino acid residues are in the favored region of Φ/Ψ space.

Miner1 is folded into two spatially distinct sub-regions: a beta rich or “Beta-Cap” domain and a helical 2Fe-2S binding or “Cluster-Binding” domain (Fig. 3B). The beta rich domain contains a strand swap from opposite ends of the primary sequence to form the Beta-Cap structure. This domain contains twenty-eight residues within beta-strands with two antiparallel strands coming from one protomer and the third parallel coming from the other (Fig. 3B). These two strand-swapped sheets pack together to form the Beta-Cap sandwich domain and form the narrowest part (~ 15 Å across) of the structure (Fig. 3B). The structure confirms the presence of two 2Fe-2S clusters expected from the optical spectrum (Fig. 2). These clusters are separated by approximately 16 Å (center-to-center) within the larger helical Cluster-Binding domain (~ 30 Å across) (Fig. 3B). A structural similarity search using the DALI server [9] revealed that this fold shows significant similarity only to the recently determined new structural “NEET” fold of mitoNEET [6; 10; 11]. This is the first example of another protein that shares the “NEET” fold.

Structure of the 2Fe-2S Clusters

The Cluster binding domain consists of the sequences Asp68-Val83 and Cys99-Asn124 on each protomer (Fig. 3B). Each 2Fe-2S cluster is cradled by a relatively short polypeptide chain from Cys99-Gly112. This segment contains the three coordinating Cys ligands (Cys99, Cys101, Cys110) and the single coordinating His ligand (His114). His114 is near the N-terminus of the α-helix within the Cluster-Binding domain (Ala113-Thr121) (Fig. 3).

Cys110 and His114, which coordinate the outermost Fe, are solvent accessible as illustrated in Figure 4 by their semitransparent surfaces. In contrast, Cys99 and Cys101, which coordinate the innermost Fe, are buried within the structure (Fig. 4). Located sequentially between the innermost Cys ligands is Arg100. It forms interprotomer interactions near the 2Fe-2S clusters. Its guanidium group forms a direct interprotomer hydrogen bond with the amide side chain of Asn84 of the other protomer. In addition, Arg100 interacts with the backbone oxygens of Cys99 and Pro108 of the other protomer via an internal water molecule (Fig. 4) locking Pro108 into a Cis conformation.

The Proton-Coupled Redox Potential of the 2Fe-2S clusters of Miner1 and its Paralog mitoNEET

A property of Miner1 that relates to possible redox activity is its redox potential E_m. The E_m values of both Miner1 and mitoNEET, *i.e.* $[2Fe\text{-}2S]^{2+}/[2Fe\text{-}2S]^{1+}$, were measured spectroscopically by the change in visible absorbances that occur upon reduction (Fig. S3). The fraction oxidized was plotted as a function of the measured ambient redox potential (Fig. S3) and fitted by the Nernst equation as described [12] yielding an E_m of ~ 0 mV (± 10 mV) at pH 7.5 for both Miner1 and mitoNEET.

In order to determine the influence of charges and titratable groups on E_m, the pH dependence was measured. The E_m values of both Miner1 and mitoNEET are pH dependent from pH 7.5 to 10.0 decreasing 50 mV per pH unit (Fig. 5A). The observed dependence shows the reduction is proton-coupled, which is often of functional relevance [13].

Drastic difference in the Half-lifes of the 2Fe-2S Clusters of Miner1 and mitoNEET

Investigations of the release of the 2Fe-2S clusters can provide information on key interactions between the clusters and the protein. The half-life of the 2Fe-2S clusters was determined from monitoring the cluster absorbance from 320nm to 600 nm as a function of time at 35°C (Fig. S4). A half-life of 700 minutes (pH 7.1) was determined from the observed signal change as a function of time. Surprisingly, given the similar fold, Miner1 was 10-fold less stable than mitoNEET [14] (Fig. 5B). In contrast, Miner1 was more stable at pH 5.3 (Fig. S4). In addition, the decay is more non-exponential suggesting a more complex unfolding energy landscape [15]. To further explore differences, we performed a more detailed investigation of the stability as a function of pH.

Investigation of the stability as a function of pH provides additional information on interactions between titrating (charged) residues and the cluster. In contrast to mitoNEET, the lifetime for Miner1 varies by only ~5-fold from pH 5.3 to 7.1 compared to ~300-fold for mitoNEET (Fig. 5B). Thus, the release of the 2Fe-2S clusters of Miner1 is orders of magnitude less sensitive to pH as those of mitoNEET.

Prominent Differences in the Charge Distribution of Miner1 and mitoNEET and in the Packing of the Beta-Cap Domain

The two proteins display prominent differences in the distribution of charges. Overall Miner1 has both fewer charged (Asp and Lys) and His residues (Fig. 6B). The homologous sites of polar Asn87 and apolar Leu93 and Leu120 in Miner1 are acidic (Asp61, Asp67 and Asp93) in mitoNEET. Other differences include (i) polar Thr106 in Miner1 replaced with a basic Lys79 in mitoNEET, (ii) acidic Glu85 by neutral Ala59, and (iii) Lys74 and Asn84 by His48 and His58. These changes result in a more positively charged and soluble domain for Miner1.

The similarities and differences in the properties of Miner1 and mitoNEET are evident when the two structures are superimposed (Fig. 6). Miner1 is the second known member of the family first established by the determination the mitoNEET structure [6; 10; 11]. (Fig. 6). The Cluster-Binding domains of Miner1 and mitoNEET share the same 3Cys-1His 2Fe-2S coordination and are structurally the same within uncertainty (rmsd ~ 0.3, pdb ID 2QH7 [6]).

However, superposition of the dimeric structures reveals significant differences in the outermost strands. The backbone rmsd of the Beta-Cap domain is ~ 1.1 Å, c.a. 4-fold greater than that of the cluster binding domain (Fig. 6A). These differences result in a more open “V” shape appearance in the Beta-Cap of Miner1. As an additional test of the significance of this apparent difference, we superimposed the protomor structures of Miner1 and mitoNEET (Fig. 7A). Strikingly, the central strand along with the Cluster -Binding domain of the protomers

are superimposable. However, the outer strands (circled) are shifted with respect to one another. Interestingly, Miner1 has an amino acid insertion at the top of the Beta-Cap domain (Thr 94 Fig 7 highlighted) that appears to act as a spacer extending the distance between the central and the outer strand. In addition, several key variations in aromatic residues (Phe60/Ile86 and Phe82/Ala109) not only create differences in side chain orientation, but also appear to affect the position of Tyr 71/Tyr98, with a relative displacement of 2.2Å.

Discussion

We report here the crystal structure determined to 2.1 Å resolution of the ER protein Miner1. We show that contrary to its original annotation, it contains redox active 2Fe-2S clusters with an E_m ~ 0mV at pH 7.5. Miner1 is a member of the novel 2Fe-2S CDGSH protein family and the first FeS protein localized to the ER. Mis-splicing of the mRNA that codifies this protein is causative in the genetic disease Wolfram Syndrome 2 (WFS2). FeS proteins participate in many types of biochemical reactions, the most predominantly characterized are oxidation-reduction reactions, but they also participate in Fe-S cluster assembly and gene expression regulation [16; 17; 18; 19]. Although not yet determined *in vivo*, Miner1 has biophysical properties necessary to participate in the functions that play a vital role in homeostasis required for proper health and longevity. The importance of Miner1 in cellular health is evidenced in the deleterious effects of its absence in WFS2 and knockout mice [1; 2]. The potential role this protein plays in human health and defense against environmental stresses is suggested by the fact that patients with WFS2 can live to 15 years before becoming symptomatic.

Miner1 is the first 2Fe-2S protein found in the ER

Miner1 was identified as one of a small family of proteins that share the CDGSH sequence domain [4]. Based on strong perinuclear staining and its localization to a lacy network in V5 epitope studies performed in transiently expressed COS-7 cells, Wiley *et al.* suggested that Miner1 localizes to the ER [4]. Amr *et al.* subsequently confirmed this suggestion in mouse P19 cells in which N-FLAG tagged Miner1 colocalized with calnexin, a known ER marker [1]. Taken together with our structural studies (Fig. 3), Miner1 is to our knowledge the first 2Fe-2S containing protein localized to the ER membrane.

Proton-Coupled Redox Activity of Miner1

One of the best characterized functions of FeS proteins is their role in redox reactions. A primary property that relates to this function is the redox potential E_m. The E_m of Miner1 and mitoNEET were measured *via* equilibrium titration to be essentially the same at ~ 0 mV at pH 7.5. The similarity of their E_m values is expected as both Miner1 and mitoNEET have nearly superimposable structures of the Cluster binding domains which includes the rare 3 Cys-1 His coordination. The E_m values varies by −50mV/pH unit indicating that the reductions are proton-coupled (Fig. 5A). Since both Miner1 and mitoNEET display the same behavior, the site of protonation is also likely the same. Given the magnitude of the change in redox potential (> 150 meV), the protonation site must be located near the 2Fe-2S cluster. In addition to the inorganic sulfide of the cluster, the 2Fe-2S clusters share ligation by Cys110 and His114 and interact with the nearby Asp111 and Ser104. Further localization of the proton requires additional investigations.

The most common redox-active motifs for 2Fe-2S proteins are ferredoxin-like whose clusters are coordinated by 4 Cys and Rieske-like whose clusters are coordinated by 2 Cys and 2 His. The Fd-like proteins tend to have negative E_m (~ − 300 mV) and the Rieske-like positive E_m (~ + 300 mV) although some can be in the same range as Miner1 [17]. Miner1 and mitoNEET have similar redox potentials as with known electron transfer species such as cytochrome b and quinones [20; 21]. Thus, their potentials are within the physiological range consistent with

Miner1 and mitoNEET participating in electron transfer or oxidation/reduction reactions in the cell.

Different pH Sensitivities of the 2Fe-2S Clusters of Miner1 and mitoNEET

Another known functional role for FeS proteins is cluster assembly and transfer [19]. The Miner1 family shares the unusual 3Cys-1His coordination with only one other known protein structure – that of an IscU D38A mutant from a hyperthermophilic bacteria [22], a protein that participates in cluster assembly. In order for this function to be plausible for Miner1, the Fe-S cluster must be easily transferable or labile. The measured lifetime of the 2Fe-2S clusters of Miner1 was ~ 10-fold shorter at pH 7.1 than that of mitoNEET [4]. This lability is accelerated by orders of magnitude in cellular extracts (data not shown), suggesting a possible role of Miner1 in FeS cluster assembly and/or transfer.

Surprisingly, given the high structural similarity of Miner1 and mitoNEET, the lability of the two proteins displayed drastically different pH dependences. Whereas the lability of Miner1 varied by only ~5-fold from pH 5.3 to 7.1, mitoNEET varied ~ 300-fold over the same range (Fig. 5). This difference in the lability is likely due to differences in the charged or titratable groups of the proteins. A site specific comparison revealed seven differences between the proteins (Figure 6) – Lys74, Asn84, Glu85, Asn87, Leu93, Thr106 and Leu120. One or more of these changes are likely responsible for the altered pH sensitivity.

Miner1, ER Function and Health and Disease

Miner1 is targeted to the ER membrane [1; 4], the organelle in which lipid synthesis, protein folding and protein maturation take place. A number of post-translational modifications are performed here including lipidation, hydroxylation, glycosylation, methionine and cysteine oxidation [23; 24]. The ER also participates in quality control by facilitating the recognition and targeting of aberrant proteins for degradation [25]. When its capacity is exceeded, a signaling network called the unfolded protein response is activated [24]. The redox ability of Miner1 could allow it to participate in protein modification and possible ER stress responses.

Recent studies on the tethering of the ER and mitochondria *via* the protein mitofusin indicate that a direct interaction between the organelles is essential for Ca^{2+} transfer and cellular function [26; 27]. Increasing evidence also links altered communication between the ER and mitochondria to apoptosis and disease [28; 29; 30]. Mitochondrial-ER crosstalk is implicated in type 2 diabetes [23; 31; 32; 33; 34]. Interestingly, Miner1 is situated on the surface of the ER and mitoNEET is on the surface of the OMM. The similarities in their E_m indicate that they would respond to similar redox stimuli and could possibly communicate through electron transfer thus providing a means of ER-mitochondrial crosstalk.

Proper biological function of Miner1 is necessary for cellular health, as the absence of Miner1 has deleterious effects such as WFS2 [1] or decreased longevity [2] (Fig. 1). The similarities of Miner1 with its paralog mitoNEET also strengthen the link between proper function of this novel family of 2Fe-2S proteins and general health. Thus, further investigation of the interplay between the functional and biophysical properties of this family are anticipated to advance our understanding of these complex mechanisms involved in health and metabolic disease.

Materials and Methods

Expression and Purification

The soluble domain of miner1 (residues 57-135) (cDNA purchased from Open Biosystems) was amplified by PCR and subcloned into bacterial expression vector pET28a(+) (Novagen) containing an N-terminal, thrombin cleavable his-tag. The C92S mutation was made by site-

directed mutagenesis using PCR. This plasmid was transformed into BL21-RIL(DE3) (Stratagene) and grown as described [6]. Harvested cells were resuspended in binding buffer (20mM Tris-HCl pH7.9, 5mM Imidazole, 500mM NaCl). After centrifugation, the lysate was added to Ni-NTA resin. After 10x volume wash in wash buffer (20mM Tris-HCl pH 7.9, 30mM Imidazole, 500mM NaCl), equilibrated in thrombin cleavage buffer (25mM Tris-HCl pH 8.0, 100mM NaCl, 2.5mM $CaCl_2$), and cleaved upon addition of thrombin at room temperature 16–24 hours. Miner1 was eluted with wash buffer and subsequently further purified by size exclusion chromatography (S-200 GE Healthcare) in 25mM Tris-HCl pH 8.0, 100mM NaCl. For crystallographic experiments, the protein was further purified by cation-exchange chromatography (HiTrap, GE Healthcare) as described [6].

Optical Spectroscopy and Stability Measurements

All UV-Visible absorption spectra were measured from the near UV to the near IR (250–700 nm) on a Cary50 spectrometer (Varian Inc, Palo Alto CA) equipped with at temperature controlled cell (T = 35°C) (protein concentration 10–20 μM in 25 mM Tris-HCl, pH 8.0 and 100 mM NaCl).

The stabilities of the 2Fe-2S clusters were determined from monitoring their characteristic absorbance at 460nm as a function of time following dilution of the protein into the assay buffer (~20 μM protein in 100mM buffer at 35°C) (Fig. S3). The following buffers were used at the pH indicated: Tris-HCl at pH 7.1 and 6.8 and bis-Tris-HCl at pH 6.3, 5.8 and 5.3. Both the buffer and the protein were filtered prior to the start of the measurement and a layer of 100% paraffin oil was placed over the solution to minimize evaporation. The half life, corresponding to decay by 50% was determined at each pH.

Redox Measurements

The reduction state was determined by monitoring the absorbance near 460nm with 100 μM protein in 25 mM Tris-HCl pH 7.5 and 100 mM NaCl at 25°C using a quartz cuvette containing a side arm under positive Argon pressure (Airgas-West, San Diego CA) (Fig. S4). A Ag/AgCl dual reference and working electrode (Microelectrodes Inc, Bedford NH) was used to measure the ambient redox potential. Its calibration was checked using quinhydrone at pH 4.0 and pH 7.0 as recommended. 50 mM pH buffered dithionite (Fisher Scientific, Pittsburgh PA) was added via a Hamilton syringe to adjust the redox potential. 50 μM ubiquinone (Sigma-Aldrich), 50 μM duroquinone (Sigma-Aldrich), 100 μM menadione (Sigma-Aldrich), and 100 μM naphthaquinone (Sigma-Aldrich) were added to ensure efficient electron transfer between the solution components and the electrode. The midpoint/redox potential (E_m) was determined from a fit of the fraction oxidized to the Nernst equation (A= A_{ox}/{1 + 10 ^ [(E_m − E) (n/59.1 mV)]} + A_{red}) using the graphing program Origin 6.1 (OriginLab Corporation) where A_{ox} is the absorbance of the fully oxidized sample, E_m is the midpoint potential in mV, E is the measured cell potential in mV, n is the number of electrons being transferred in the redox reaction, and A_{red} is the lowest absorbance level corresponding to the fully reduced 2Fe-2S center in either native or mutant mitoNEET. Potentials were adjusted to SHE for presentation. Samples were tested for their ability to reoxidize upon exposure to ambient oxygen.

Crystallization

Crystallization was achieved as described previously for mitoNEET [6]. Final conditions were 100 mM Tris-HCl pH 8.0, 100 mM NaCl, and 15–20% PEG 3000 in the protein well, equilibrating against 100 mM Tris-HCl pH 8.0 and 30–33% PEG 3000 in the reservoir. Crystals were frozen (77 K) after a 1-min soak in 100 mM Tris-HCl pH 8.0, 40% PEG3000 and sent frozen (77 K) to SSRL in an SSRL-supplied cassette system for x-ray data collection and analysis.

X-Ray Data Collection and Structural Determination

Frozen crystals were screened using the Stanford Automated Mounter [35] operated by Blu-Ice [36]. The data were recorded using a Rayonix MX-325 CCD detector at BL9-2 and an ADSC Q315R CCD detector at BL7-1. Data were processed with XDS [37]. The structure of Miner1 was determined by MAD phasing [5; 38]. Data reduction and primary phasing at a resolution of 2.1 Å were accomplished as previously described [6].

Data Deposition

The atomic coordinates have been deposited in the Protein Data Bank, www.pdb.org (PDB ID code 3FNV; RCSB ID code rcsb050821).

Supplementary Material

Refer to Web version on PubMed Central for supplementary material.

Acknowledgments

Supported by grants from the NIH [grants GM 41637 (to M. Okamura and M.L. Paddock), and GM54038 and DK54441 (to P.A.J.)]. Students were supported by the HEME and CMG training grants. R. N. thanks the Zevi Hermann Shapira Foundation for supporting the collaborative USA-Israeli efforts. We thank Christopher L. Rife at the Joint Center for Structural Genomics for providing an automated programming script for coordinate validation, Mitch Miller at SSRL for helpful discussions on the data collection and processing and Mel Okamura for helpful discussions and support. Portions of this research were carried out at the Stanford Synchrotron Radiation Laboratory, a national user facility operated by Stanford University on behalf of the U.S. Department of Energy, Office of Basic Energy Sciences. The SSRL Structural Molecular Biology Program is supported by the Department of Energy, Office of Biological and Environmental Research, and by the National Institutes of Health, National Center for Research Resources, Biomedical Technology Program, and the National Institute of General Medical Sciences.

Abbreviations

ER
: endoplasmic reticulum

MAD
: multiwavelength anomalous dispersion

SSRL
: Stanford Synchrotron Radiation Laboratory

OMM
: outer mitochondrial membrane

References

1. Amr S, Heisey C, Zhang M, Xia XJ, Shows KH, Ajlouni K, Pandya A, Satin LS, El-Shanti H, Shiang R. A homozygous mutation in a novel zinc-finger protein, ERIS, is responsible for Wolfram syndrome 2. Am J Hum Genet 2007;81:673–683. [PubMed: 17846994]
2. Tsai, T.; Chen, Y.; Tsai, S.; Chen, Y. United States Patent Trademark Office. National Yang-Ming University, Taipei City (TW) National Health Research Institutes; Miaoli County (TW), USA: 2008. Cisd2-knockout mice and uses thereof; p. 19
3. Colca JR, McDonald WG, Waldon DJ, Leone JW, Lull JM, Bannow CA, Lund ET, Mathews WR. Identification of a novel mitochondrial protein (“mitoNEET”) cross-linked specifically by a thiazolidinedione photoprobe. Am J Physiol Endocrinol Metab 2004;286:E252–E260. [PubMed: 14570702]

4. Wiley SE, Murphy AN, Ross SA, van der Geer P, Dixon JE. MitoNEET is an iron-containing outer mitochondrial membrane protein that regulates oxidative capacity. Proc Natl Acad Sci USA 2007;104:5318–5323. [PubMed: 17376863]
5. Pahler A, Smith JL, Hendrickson WA. A probability representation for phase information from multiwavelength anomalous dispersion. Acta Crystallogr A 1990;46 (Pt 7):537–40. [PubMed: 2206480]
6. Paddock ML, Wiley SE, Axelrod HL, Cohen AE, Roy M, Abresch EC, Capraro D, Murphy AN, Nechushtai R, Dixon JE, Jennings PA. MitoNEET is a uniquely folded 2Fe-2S outer mitochondrial membrane protein stabilized by pioglitazone. Proc Natl Acad Sci USA 2007;104:14342–14347. [PubMed: 17766440]
7. Krissinel E, Henrick K. Inference of macromolecular assemblies from crystalline state. J Mol Biol 2007;372:774–797. [PubMed: 17681537]
8. Lovell SC, Davis IW, Adrendall WB, de Bakker PIW, Word JM, Prisant MG, Richardson JS, Richardson DC. Structure validation by C alpha geometry: phi,psi and C beta deviation. Proteins 2003;50:437–450. [PubMed: 12557186]
9. Holm L, Sander C. Dali - a Network Tool for Protein-Structure Comparison. Trends Biochem Sci 1995;20:478–480. [PubMed: 8578593]
10. Lin JZ, Zhou T, Ye KQ, Wang JF. Crystal structure of human mitoNEET reveals distinct groups of iron-sulfur proteins. Proc Natl Acad Sci USA 2007;104:14640–14645. [PubMed: 17766439]
11. Hou XW, Liu RJ, Ross S, Smart EJ, Zhu HN, Gong WM. Crystallographic studies of human MitoNEET. J Biol Chem 2007;282:33242–33246. [PubMed: 17905743]
12. Dutton PL. Redox Potentiometry: determination of midpoint potentials of oxidation-reduction components of biological electron transfer systems. Methods Enzymol 1978;54:411–435. [PubMed: 732578]
13. Chang CJ, Chang MC, Damrauer NH, Nocera DG. Proton-coupled electron transfer: a unifying mechanism for biological charge transport, amino acid radical initiation and propagation, and bond making/breaking reactions of water and oxygen. Biochim Biophys Acta 2004;1655:13–28. [PubMed: 15100012]
14. Wiley SE, Paddock ML, Abresch EC, Gross L, van der Geer P, Nechushtai R, Murphy AN, Jennings PA, Dixon JE. The outer mitochondrial membrane protein mitoNEET contains a novel redox-active 2Fe-2S cluster. J Biol Chem 2007;282:23745–23749. [PubMed: 17584744]
15. Onuchic JN, Kobayashi C, Miyashita O, Jennings P, Baldridge KK. Exploring biomolecular machines: energy landscape control of biological reactions. Philos Trans R Soc Lond B Biol Sci 2006;361:1439–43. [PubMed: 16873130]
16. Rees DC, Howard JB. The interface between the biological and inorganic worlds: iron-sulfur metalloclusters. Science 2003;300:929–31. [PubMed: 12738849]
17. Meyer J. Iron-sulfur protein folds, iron-sulfur chemistry, and evolution. J Biol Inorg Chem 2008;13:157–170. [PubMed: 17992543]
18. Bandyopadhyay S, Chandramouli K, Johnson MK. Iron-sulfur cluster biosynthesis. Biochem Soc Trans 2008;36:1112–9. [PubMed: 19021507]
19. Lill R, Muhlenhoff U. Maturation of iron-sulfur proteins in eukaryotes: mechanisms, connected processes, and diseases. Annu Rev Biochem 2008;77:669–700. [PubMed: 18366324]
20. Rivera M, Seetharaman R, Girdhar D, Wirtz M, Zhang X, Wang X, White S. The reduction potential of cytochrome b5 is modulated by its exposed heme edge. Biochemistry 1998;37:1485–94. [PubMed: 9484218]
21. Berg, J.; Tymoczko, J.; Stryer, L. Biochemistry. Vol. 5. W.H. Freeman; 2003. p. 734-788.
22. Shimomura Y, Wada K, Fukuyama K, Takahashi Y. The Asymmetric Trimeric Architecture of [2Fe-2S] IscU: Implications for Its Scaffolding during Iron-Sulfur Cluster Biosynthesis. J Mol Biol 2008;383:133–143. [PubMed: 18723024]
23. Rajan SS, Srinivasan V, Balasubramanyam M, Tatu U. Endoplasmic reticulum (ER) stress & diabetes. Indian J Med Res 2007;125:411–424. [PubMed: 17496365]
24. Schroder M, Kaufman RJ. ER stress and the unfolded protein response. Mutat Res 2005;569:29–63. [PubMed: 15603751]

25. Hebert DN, Molinari M. In and out of the ER: Protein folding, quality control, degradation, and related human diseases. Physiol Rev 2007;87:1377–1408. [PubMed: 17928587]
26. Merkwirth C, Langer T. Mitofusin 2 builds a bridge between ER and mitochondria. Cell 2008;135:1165–7. [PubMed: 19109886]
27. de Brito OM, Scorrano L. Mitofusin 2 tethers endoplasmic reticulum to mitochondria. Nature 2008;456:605–10. [PubMed: 19052620]
28. Zhao LH, Ackerman SL. Endoplasmic reticulum stress in health and disease. Curr Opin Cell Biol 2006;18:444–452. [PubMed: 16781856]
29. Boya P, Cohen I, Zamzami N, Vieira HLA, Kroemer G. Endoplasmic reticulum stress-induced cell death requires mitochondrial membrane permeabilization. Cell Death Differ 2002;9:465–467. [PubMed: 11965500]
30. Takuma K, Yan SSD, Stern DM, Yamada K. Mitochondrial dysfunction, endoplasmic reticulum stress, and apoptosis in Alzheimer's disease. J Pharmacol Sci 2005;97:312–316. [PubMed: 15750290]
31. Hacki J, Egger L, Monney L, Conus S, Rosse T, Fellay I, Borner C. Apoptotic crosstalk between the endoplasmic reticulum and mitochondria controlled by Bcl-2. Oncogene 2000;19:2286–2295. [PubMed: 10822379]
32. Ozcan U, Cao Q, Yilmaz E, Lee AH, Iwakoshi NN, Ozdelen E, Tuncman G, Gorgun C, Glimcher LH, Hotamisligil GS. Endoplasmic reticulum stress links obesity, insulin action, and type 2 diabetes. Science 2004;306:457–461. [PubMed: 15486293]
33. Nakatani Y, Kaneto H, Kawamori D, Yoshiuchi K, Hatazaki M, Matsuoka T, Ozawa K, Ogawa S, Hori M, Yamasaki Y, Matsuhisa M. Involvement of endoplasmic reticulum stress in insulin resistance and diabetes. J Biol Chem 2005;280:30648–30648.
34. Marciniak SJ, Ron D. Endoplasmic reticulum stress signaling in disease. Physiol Rev 2006;86:1133–1149. [PubMed: 17015486]
35. Cohen AE, Ellis PJ, Miller MD, Deacon AM, Phizackerley RP. An automated system to mount cryo-cooled protein crystals on a synchrotron beamline, using compact sample cassettes and a small-scale robot. J Appl Crystallogr 2002;35:720–726.
36. McPhillips TM, McPhillips SE, Chiu HJ, Cohen AE, Deacon AM, Ellis PJ, Garman E, Gonzalez A, Sauter NK, Phizackerley RP, Soltis SM, Kuhn P. Blu-Ice and the Distributed Control System: software for data acquisition and instrument control at macromolecular crystallography beamlines. J Synchrotron Radiat 2002;9:401–406. [PubMed: 12409628]
37. Kabsch W. Automatic Processing of Rotation Diffraction Data from Crystals of Initially Unknown Symmetry and Cell Constants. J Appl Crystallogr 1993;26:795–800.
38. Terwilliger TC, Berendzen J. Automated MAD and MIR structure solution. Acta Crystallogr D Biol Crystallogr 1999;55:849–861. [PubMed: 10089316]
39. De Lano W, Lam J. PyMOL: A communications tool for computational models. Abstr Pap Am Chem Soc 2005;230:u1371–u1372.

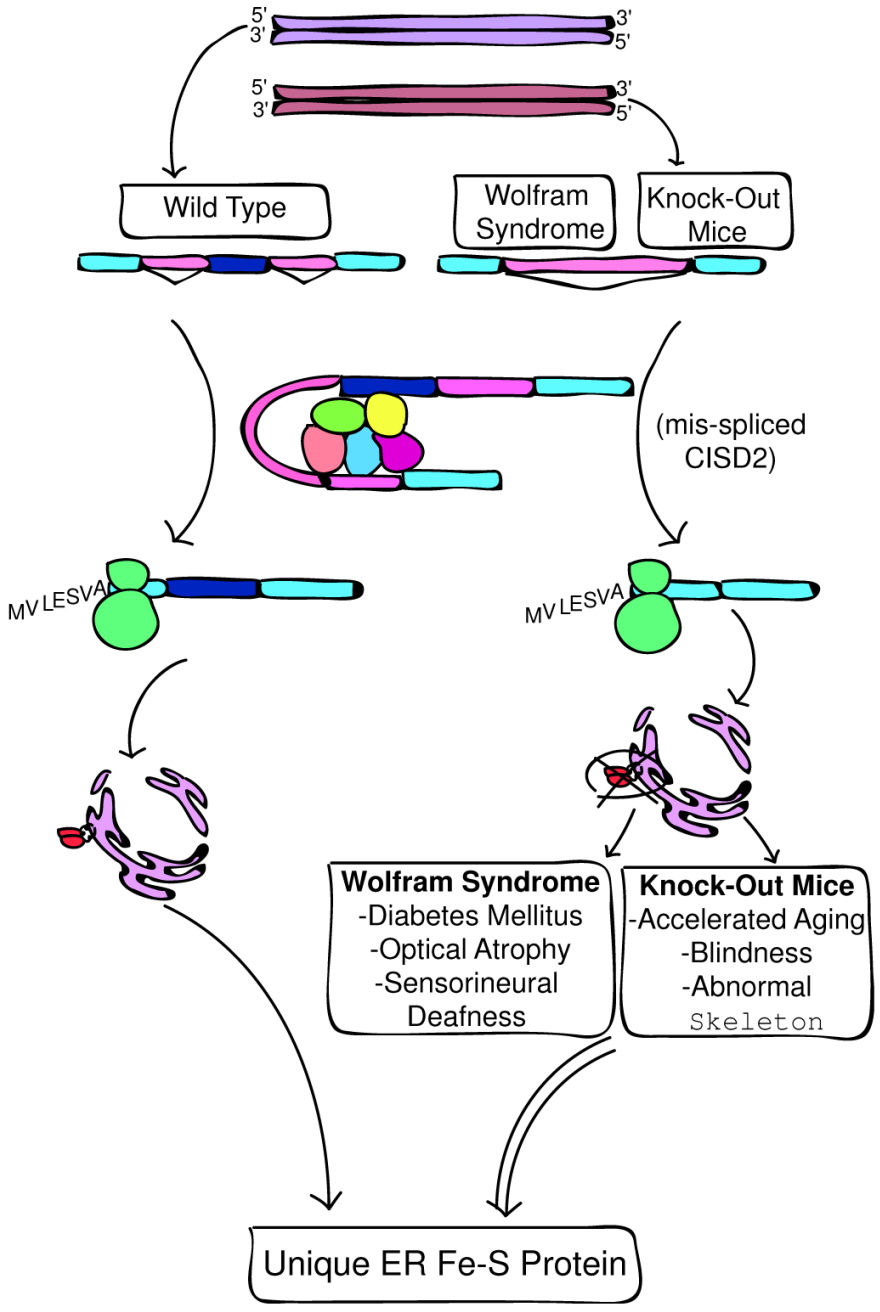

Figure 1. Elimination of functional Miner1 protein leads to multiple symptoms in both human and mice models

CISD2, shown at the top, codifies an endoplasmic reticulum (ER) protein Miner1 (left side). Amr *et al.* recently showed that Wolfram Syndrome 2 is attributed to a single base pair conversion in the CISD2 gene [1]. This mutation causes a splicing error that completely eliminates exon2 and creates a premature stop codon in exon 3 (right side). For these reasons, 75% of the protein sequence is not translated [1] and no Miner1 is properly assembled in the ER (lower part of right side). The absence of this protein causes a wide range of symptoms in WFS2 patients, including diabetes mellitus and optical atrophy [1]. In an independent study, CISD2 knockout mice were constructed with a coding error that causes incorrect splicing,

resulting in an inoperative gene [2]. Knock-out mice are also symptomatic, with similar signs of early aging and optical atrophy [2].

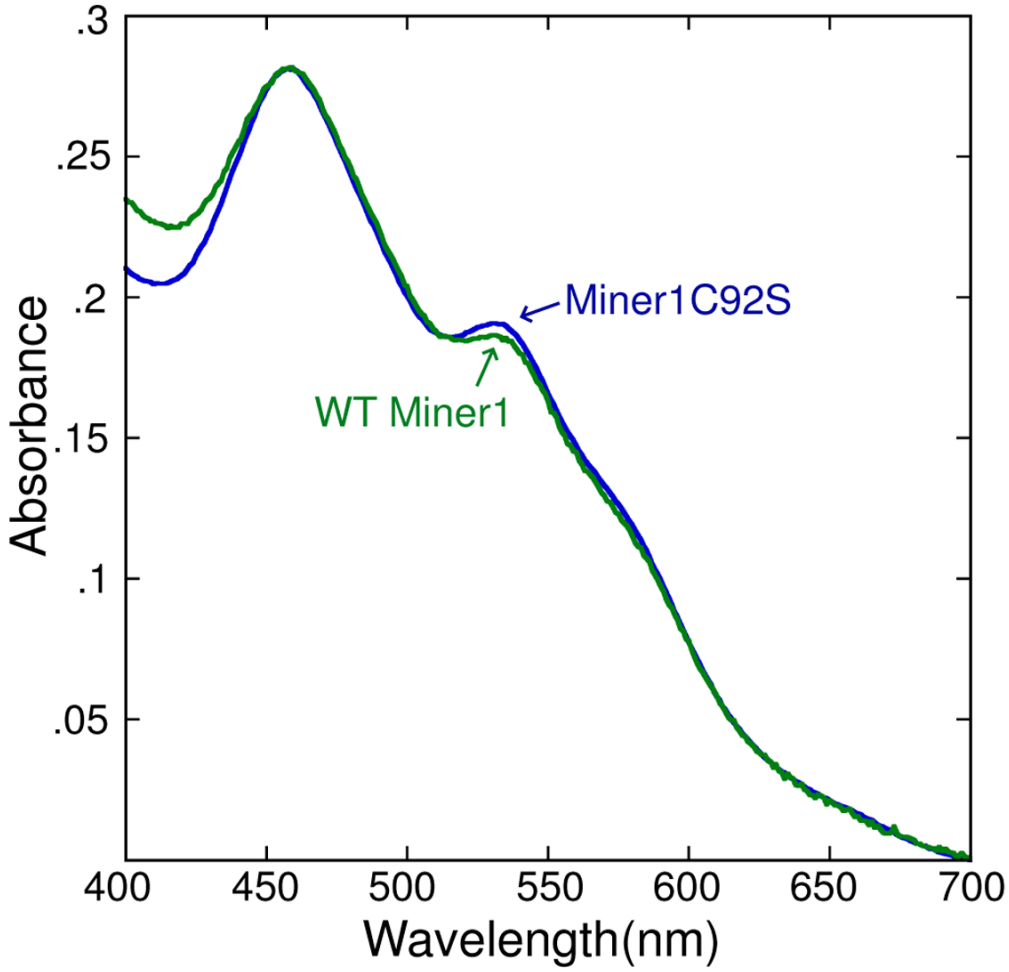

Figure 2. Miner1 (C92S) has essentially the same UV-Vis spectrum as WT Miner1

Both Miner1 (green) and Miner1 (C92S) (blue) show the same 2Fe-2S absorbance peaks at 460nm and 530nm. Thus, the C92S point mutation does not significantly affect the Miner1 optical signature.

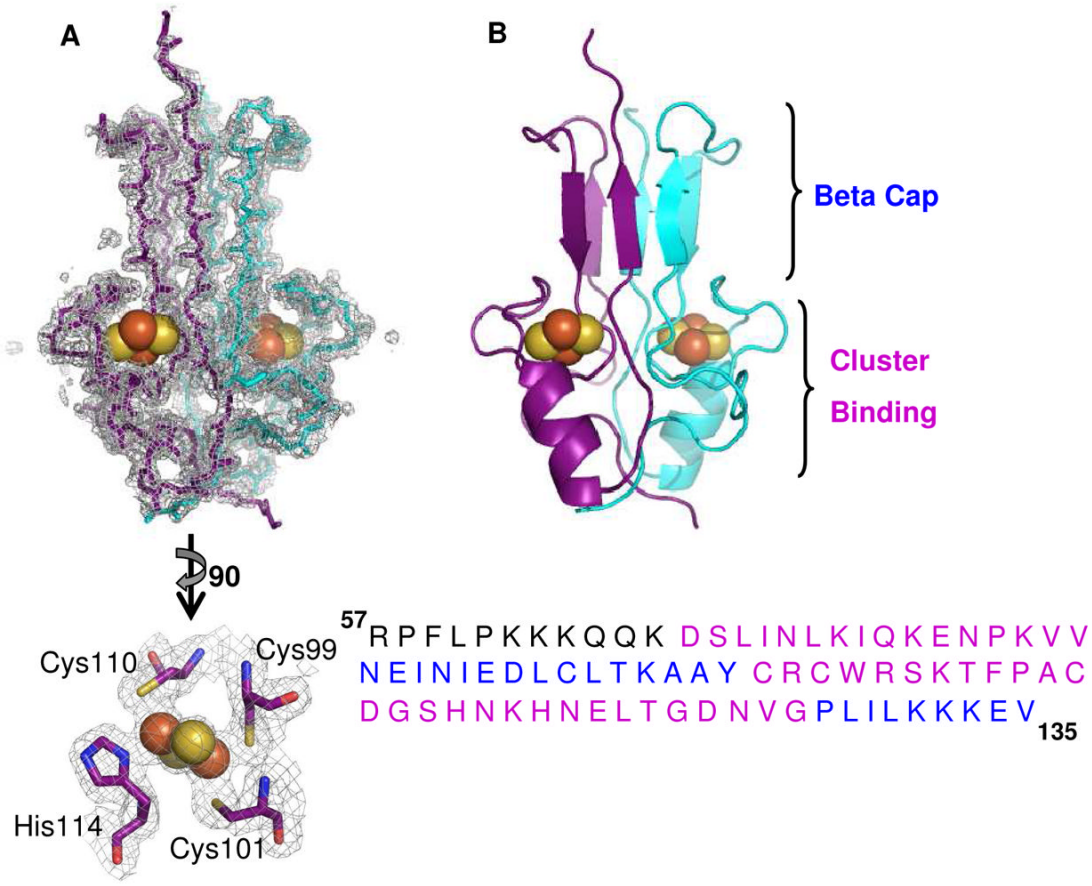

Figure 3. Structural organization and domain topology of dimeric Miner1

(A) (Upper) The backbone tracing of homodimeric Miner1. Protomers are colored in purple and cyan together with the observed 2Fo-Fc electron density (grey) map contoured at 1.5 σ. A 2Fe-2S cluster is present in each protomer (Fe - red spheres, S – yellow). The two protomers are related by a dyad axis along the vertical direction in the plane of the paper (see arrow). (Lower) An expanded view of one 2Fe-2S cluster (rotated ~90° counterclockwise along the dyad axis) showing the cluster and iron ligands (O colored red, N blue and C green) and the corresponding observed 2Fo-Fc electron density (grey) map contoured at 2.0σ. The amino acid ligands are indicated. (Rendered with Pymol, [39]) **(B)** Ribbon diagram highlighting the two domains and protomer interactions within the Miner1 homodimer: a six stranded beta sandwich forms an intertwined **beta cap** and a larger **cluster binding** domain carries two 2Fe-2S clusters (one per protomer). Below is the amino acid sequence of the construct. Coded segments contributing to each domain are highlighted on the primary sequence with magenta for the beta cap and blue for the cluster binding domains. The 2Fe-2S binding cradle is located sequentially between two parts of the beta cap domains.

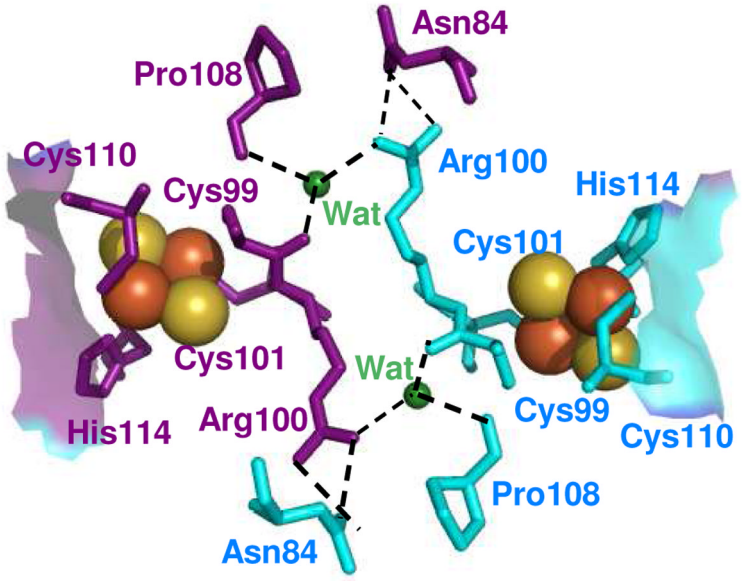

Figure 4. The 2Fe-2S cluster binding cradle

View of the 2Fe-2S cluster (Fe as brown and S as yellow spheres) from a perspective rotated ~90° along an axis perpendicular to the dyad axis from that shown for the cluster binding site in the panel A of Figure 3. The amino acids belonging to the individual protomers are shown in purple and cyan, respectively. The two 2Fe-2S cradles are related to each other via a 180° rotation along the dyad symmetry axis of the dimer located approximately perpendicular to the page. Cys110 and His114 bind the outermost Fe while the innermost Fe is bound by Cys99 and Cys101 (as indicated). The solvent accessible His114 is located at the end of the prominent alpha helix in the Cluster Binding domain (Figure 3). Two additional residues, Arg100 and Asn84 form an interprotomer bifurcated hydrogen bond within the interior of the protein dimer. Each Arg100 also forms a potential hydrogen bond with one of two internal water molecules shown as green spheres and labeled as Wat. These Wat form additional interprotomer hydrogen bonds with the backbone oxygen atoms of Cys99 and Pro108.

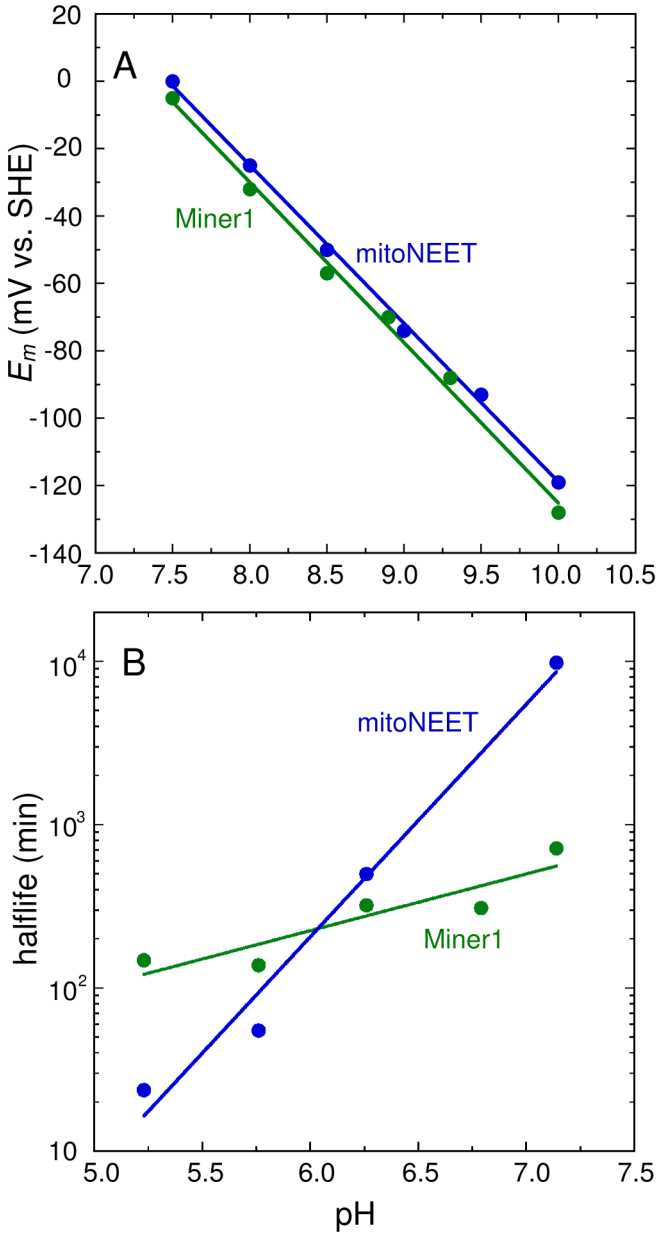

Figure 5. Redox potential and Stability of the 2Fe-2S clusters of Miner1 and mitoNEET

(A) pH dependence of the redox potentials (E_m) of Miner1 and mitoNEET. Both Miner1 and mitoNEET display pH dependent E_m values from pH 7.5 to 10.0 that decrease 50 mV per pH unit indicating that the reduction is proton-coupled **(B).** pH dependence of the 2Fe-2S cluster stabilities of Miner1 and mitoNEET. The halflife for Miner1 is orders of magnitude less pH dependent varying by only ~5-fold from pH 5.3 to 7.1 compared to an ~300-fold change for mitoNEET

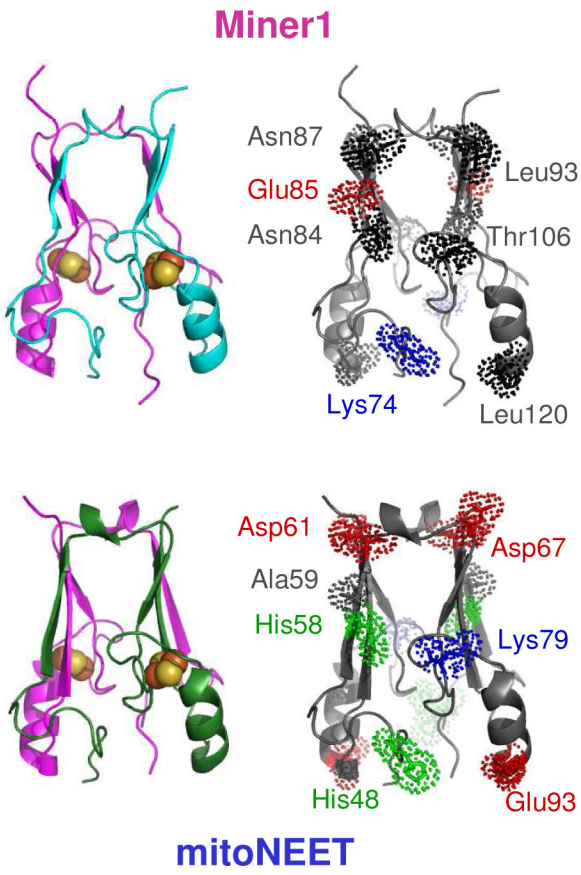

Figure 6. Differences in the backbone and charge distributions of Miner1 and related mitoNEET structures

(A) Shown are ribbon diagrams of Miner1 and mitoNEET [6] from a perspective rotated 90° along the dyad axis from that in Figure 3B. The two proteins share a similar fold, previously termed the NEET fold. The cluster binding domains are nearly superimposable. In contrast, there are differences greater than the uncertainty in the beta cap domains with Miner1 appearing more open near the top forming more of a "V" shape. **(B)** Highlighted are the sites were amino acid differences between Miner1 and mitoNEET result in either a change in a charged or a titratable group. In most cases, the neutral residues in Miner1 are replaced with charged groups or His in mitoNEET resulting in a more positively charged soluble domain for Miner1. Ribbon backbone is shown in grey, neutral residues are in black, negative red, positive blue and His green. Sites of changes are labeled on only one of the protomers for simplicity.

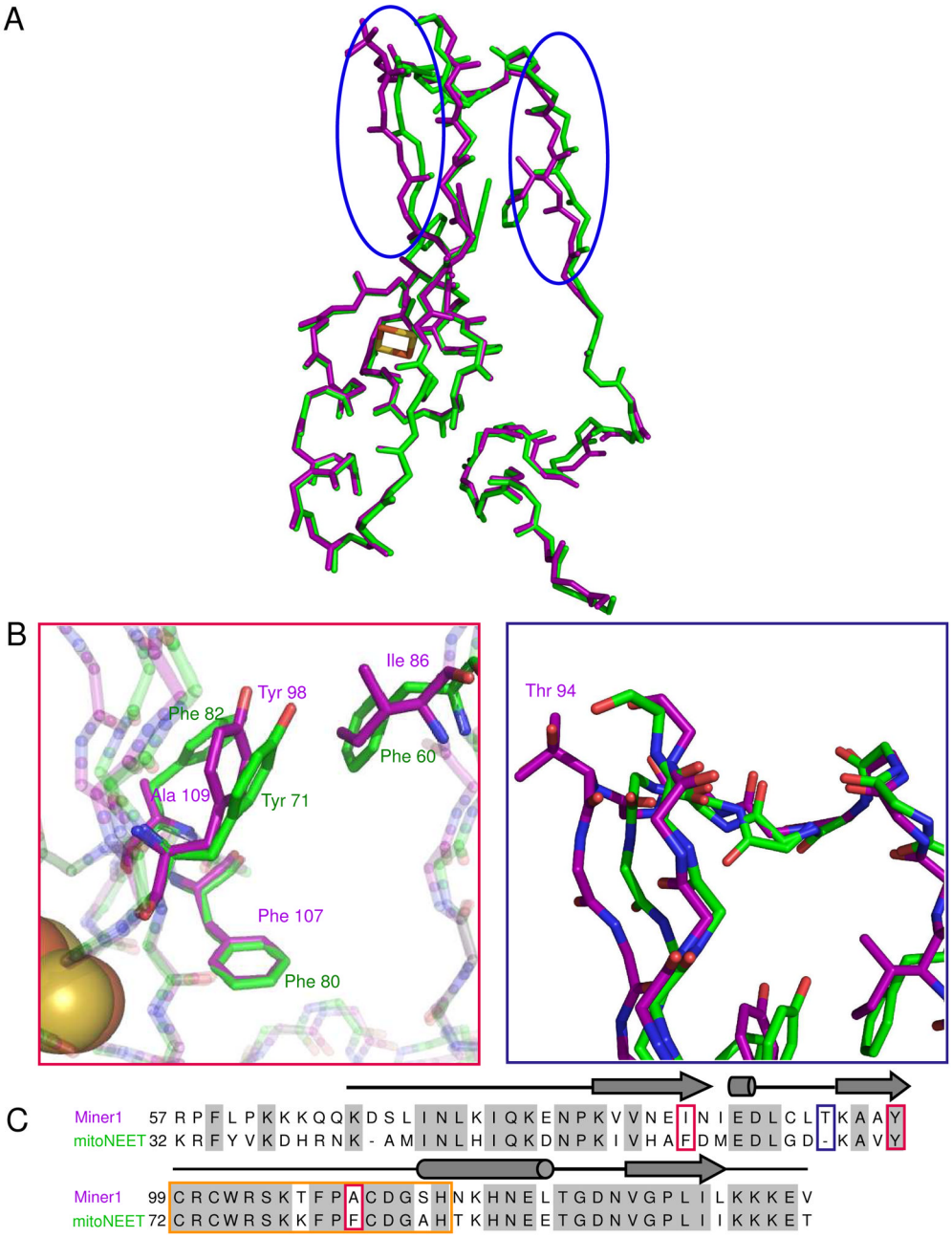

Figure 7. Protomer superposition of Miner1 and mitoNEET highlighting distinct backbone and side chain conformations

(A) Shown is the backbone superposition of Miner1 protomer A on mitoNEET protomer A. Specific side chains showing different conformations are also indicated; the region around them is expanded in part B. The 2Fe-2S centers are essentially identical in each superposition and are shown in red and yellow spheres for the Fe and S, respectively. The backbones of the two proteins are nearly indistinguishable in the lower Cluster Binding domain. **(B)** The largest difference in the backbone occurs in the local vicinity of an additional amino acid in Miner1, Thr94 (blue box). Side chain differences in the Beta-Cap domain occur near Ile88 and Ala109 of Miner1 that correspond to Phe60 and Phe82 of mitoNEET. Tyr98 located in the vicinity is

displaced from the corresponding Tyr71 of mitoNEET (red box). **(C)** Sequence alignment of Miner1 and mitoNEET. Changes to side chains shown in B are boxed in blue and red. The 16 amino acid cluster binding motif is boxed in orange. Secondary structures are indicated above the sequences by thick arrow for beta strand and cylinder for helices.

Table 1

Summary of crystal parameters, data collection, and refinement statistics for Miner1

Space Group		**$P2_12_12_1$**	
Unit cell dimensions	a=49.90 Å	b=48.58 Å c=74.10 Å	α=β=γ=90°
Data Collection	λ_1FeMAD	λ_2FeMAD	λ_3FeMAD
Wavlength (Å)	1.7418	1.3624	1.7372
Resolution Range (Å)	40.89-2.25	48.56-2.10	48.56-2.25
No. of Observations*	197,570(28,295)	244,886(36,669)	197,223(28,261)
No. of Unique Reflections*	7347(1025)	9047(1288)	7349(1024)
Completeness (%)*	98.9(97.6)	99.4(98.7)	98.9(97.5)
Mean $I/\sigma(I)$ *	23.2(6.40)	24.9(10.8)	23.8(7.3)
R_{symm} on I (%)*	12.1(89.5)	10.9(52.8)	11.7(79.2)
Model and Refinement Statistics			
Data Set Used	λ_2		
Cutoff Criteria	$\|F\| > 0$		
Resolution Range (Å)	37.1-2.10		
No. of reflections (total)	9013†		
No of reflections (test)	450		
Completeness (% total)	99.2		
Mean $I/\sigma(I)$ *	17.6(10.8)		
R_{symm} on I (%)*	10.3(52.8)		
R_{cryst}	17.0		
R_{free}	21.6		
Stereochemical Parameters			
Restraints (RMS observed)			
Bond Angle, °		1.86	
Bond length, Å		0.013	
Average isotropic B-value, $Å^2$		27.58	
ESU based on R_{free}, Å		0.164	

ESU, estimated overall coordinate error. *R*symm = $\Sigma|I_i - \langle I_i \rangle|/\Sigma I_i$ where *Ii* is the scaled intensity of the *i*th measurement and $\langle I_i \rangle$is the mean intensity for that reflection. $R_{cryst} = \Sigma|F_{obs}| - |F_{calc}|/\Sigma|F_{obs}|$ where F_{calc} and F_{obs} are the calculated and observed structure factor amplitudes, respectively. $Rf_{ree} = R_{cryst}$, but for 5.0% of the total reflections chosen at random and omitted from refinement.

*Highest-resolution shell in parentheses.

†Typically, the number of unique reflections used in refinement is less than the total number that were integrated and scaled. Reflections are excluded due to systematic absences, negative intensities, and rounding errors in the resolution limits and cell parameters.